2011

Improving the measurement performance for a self-mixing interferometry-based displacement sensing system

Yuanlong Fan

Yanguang Yu
University of Wollongong, yanguang@uow.edu.au

Jiangtao Xi
jiangtao@uow.edu.au

Jose Chicharo

Improving the measurement performance for a self-mixing interferometry-based displacement sensing system

Abstract

Approaches that are, to our knowledge, novel, are proposed in this paper to improve the accurancy performance of self-mixing interferometruy (SMI). First the characteristics associated with signals observed in SMI systems are studied, based on which a new procedure is proposed for achieving accurate estimation of the laser phase.

Disciplines

Physical Sciences and Mathematics

Publication Details

Y. Fan, Y. Yu, J. Xi & J. F. Chicharo, "Improving the measurement performance for a self-mixing interferometry-based displacement sensing system," Applied Optics, vol. 50, (26) pp. 5064-5072, 2011.

Improving the measurement performance for a self-mixing interferometry-based displacement sensing system

Yuanlong Fan, Yanguang Yu,* Jiangtao Xi, and Joe F. Chicharo

School of Electrical, Computer and Telecommunications Engineering, University of Wollongong, Northfields Avenue, Wollongong, New South Wales 2522, Australia

*Corresponding author: yanguang@uow.edu.au

Received 31 March 2011; revised 5 July 2011; accepted 19 July 2011; posted 25 July 2011 (Doc. ID 144931); published 5 September 2011

Approaches that are, to our knowledge, novel, are proposed in this paper to improve the accuracy performance of self-mixing interferometry (SMI) for displacement measurement. First, the characteristics associated with signals observed in SMI systems are studied, based on which a new procedure is proposed for achieving accurate estimation of the laser phase. The studies also revealed the reasons for the inherent errors associated with the existing SMI-based techniques for displacement measurement. Then, this paper presents a new method for estimating the optical feedback level factor (denoted by C) in real time. Combining the new algorithms for estimating the laser phase and updating C value, the paper finally presents a novel technique for displacement measurement with improved accuracy performance in contrast to existing techniques. The proposed technique is verified by both simulation and experimental data.

OCIS codes: 120.3180, 280.3420, 140.5960.

1. Introduction

As an emerging sensing technique, self-mixing interferometry (SMI) has attracted extensive research effort in the past two decades. Potential applications of SMI include measurement of various metrological quantities, such as velocity, vibration, displacement, and absolute distance [1–4]. In contrast to other interferometric sensing systems, an SMI-based sensing system is characterized by impact structure and simple implementation. A basic SMI structure consists of a laser diode (LD), a microlens, and a moving target, which form an external cavity of the LD. With a small portion of light backscattered or reflected by the moving target reentering the LD cavity, both the amplitude and frequency of the LD power are modulated [5]. This modulated LD power is detected as a self-mixing signal (SMS), which can be used to measure the abovementioned metrological quantities associated with the target.

Displacement measurement is one of important applications of SMI-based sensing. In 1995, Donati *et al.* [6] developed a fringe counting method based on the fact that each fringe on an SMS waveform corresponds to a half-wavelength shift of a moving target. The method is simple but only achieves the resolution of a half-wavelength for displacement measurement. This sensing scheme has been improved by different methods in terms of measurement accuracy [7–9]. In 1998, Servagent *et al.* [8] found that the fringe shape of an SMS is sawtooth-like under moderate feedback level. Thus, they performed linear interpolation processing on each fringe of an SMS and achieved a resolution of $\lambda_0/12$ (λ_0 is the wavelength of the laser used in an SMI). In 2005, Guo *et al.* [9] proposed a sinusoidal phase modulating technique by placing an electro-optic modulator on an SMI basic structure. With this setup, displacement information can be extracted by analyzing the initial phase of an SMS using Fourier

transform. This method can reduce the measurement error to 10 nm ($\lambda_0/65$). However, this method is only suitable for the case of weak feedback. In order to achieve higher resolution, a phase unwrapping approach has become attractive, which tries to establish a unique mapping from an SMS waveform and the laser phase, and the later will give an accurate displacement. In 1997, Merlo and Donati [7] first proposed a phase unwrapping algorithm based on an SMI sensing model. The reconstruction accuracy of displacement is on the order of tens of nanometers ($\lambda_0/67$). However, the reconstruction algorithm in [7] only works for a weak feedback level. Besides, two parameters are required by the algorithm in [7], namely the optical feedback level factor (denoted C) and the linewidth enhancement factor (LEF) α. In 2005 and 2006, Plantier *et al.* [10] and Bes *et al.* [11] presented a new reconstruction algorithm suitable for moderate feedback level with $C > 1$. This method provides a real-time measurement of the C value using an optimization criterion based on the instantaneous power of the reconstructed signal discontinuities [10]. However, the method is quite time-consuming [12] and vulnerable to noises. In 2009, based on the work in [10] and [11], Zabit *et al.* [13] proposed an improved algorithm by introducing the adaptive transition detection method. The method in [13] can detect all SMS fringes by automatically converging to the optimal threshold. The improved algorithm can work for both weak and moderate feedback levels.

Based on careful investigation of the existing reconstruction algorithms, we found that none of them is able to perfectly reconstruct displacement from an SMS due to an inherent measurement error in these methods. The influence of the error can be seen from the results presented in Figs. 2 and 3 in [7], Figs. 3 and 8 in [10], and Fig. 9 in [13].

In this paper, we will study the features of the fringe shape of an SMS in different scenarios, based on which we will present a novel algorithm that can accurately extract displacement information from an SMS. The studies also reveal the reasons for the abovementioned inherent measurement error associated with existing displacement reconstruction algorithms. The paper is organized as follows. In Section 2.A, we introduce the basic measurement principle of an SMI-based sensing system. Then, the features of an SMS are analyzed in Section 2.B. In Section 2.C, the improved algorithm is derived and presented. Details of computer simulations and experiments are shown in Section 3. Finally, we conclude the paper in Section 4.

2. Novel Algorithm for SMI-Based Displacement Sensing

A. Principle of SMI-Based Displacement Sensing

The SMI-based sensing system has been studied extensively [14–17]. A widely accepted mathematical model for describing an SMS is rewritten below:

$$\phi_0(n) = 4\pi L(n)/\lambda_0, \tag{1}$$

$$\phi_F(n) = \phi_0(n) - C\sin[\phi_F(n) + \arctan(\alpha)], \tag{2}$$

$$g(n) = \cos(\phi_F(n)), \tag{3}$$

$$p(n) = p_0[1 + b \cdot g(n)]. \tag{4}$$

The physical meanings of the parameters in the above model are described in Table 1.

The above model shows that the straightforward approach to retrieving $L(n)$ from an SMS $p(n)$ is to follow the procedure $p(n) \to g(n) \to \phi_F(n) \to \phi_0(n) \to L(n)$. Note that $g(n)$ can be obtained by Eq. (4) from $p(n)$, and $L(n)$ can be obtained from $\phi_0(n)$ using Eq. (1). Hence the key part of the procedure is $g(n) \to \phi_F(n) \to \phi_0(n)$, consisting of the following two steps:

- The first step is to obtain $\phi_F(n)$ from $g(n)$. Based on Eq. (3), this can be carried out by applying inverse cosine function to $g(n)$, that is, $\phi'_F(n) = \arccos[g(n)]$. However, as the value of $\phi'_F(n)$ is wrapped within the range of $[0, \pi]$, an operation called phase unwrapping must be applied to $\phi'_F(n)$ in order to obtain the true phase $\phi_F(n)$. When $\phi'_F(n)$ increases to reach π, a step of 2π is added to the result of unwrapping operation; when $\phi'_F(n)$ decreases to reach 0, a step of 2π should be subtracted from the result of the unwrapping operation. Obviously, detection of critical points of an SMS waveform is very important, as it significantly affects the accuracy for estimation of $\phi_F(n)$ and hence the displacement as well.
- The second step is to calculate $\phi_0(n)$ from $\phi_F(n)$ using Eq. (2). In order to do this, the two parameters in Eq. (2), namely, α and C, must be available. Note

Table 1. Meaning of Parameters in Equations (1)–(4)

Parameters	Meaning
n	Discrete time index
$\phi_0(n)$	Light phase without external optical feedback
$L(n)$	Distance between the LD facet and the external target
λ_0	Emitted laser wavelength without optical feedback
$\phi_F(n)$	Light phase with external optical feedback
C	Optical feedback level factor
α	Linewidth enhancement factor (LEF)
$g(n)$	Interference function that indicates the influence of the self-mixing effect on the emitted intensity
$p(n)$	Laser power emitted by LD with feedback from external cavity
p_0	Laser power emitted by the free running LD
b	Modulation index for the laser intensity (typically $b \approx 10^{-3}$)

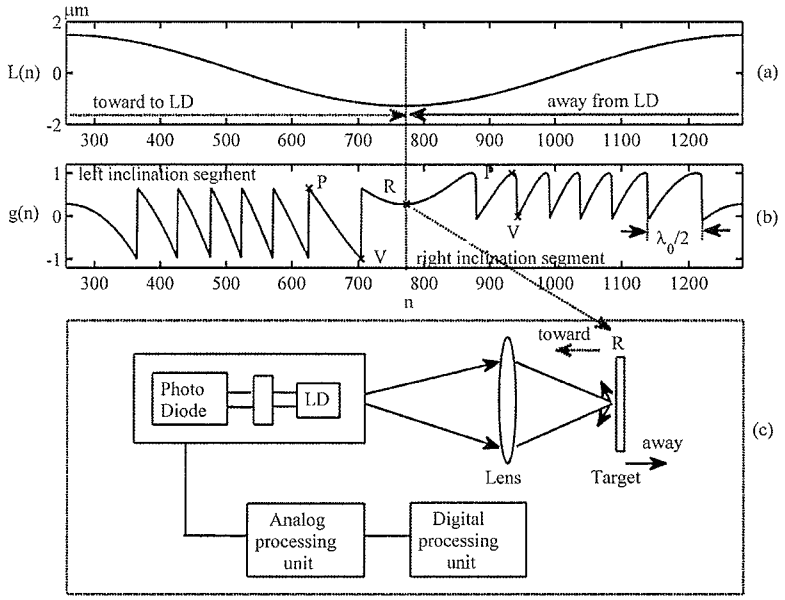

Fig. 1. SMI-based displacement sensing system and an SMS waveform. (a) Displacement $L(n)$ generated by the moving target; (b) SMS waveform with $C = 3$, $\alpha = 3$; (c) SMI structure.

that α and C are both fundamental parameters in an SMI and their measurement has also attracted a significant amount of research [16–18]. In general, α is considered an unchanged parameter for an LD, which can be measured [16–18]. However, C varies significantly during the operation of an SMI system, as reported by the experiment results in [16,18]. Therefore, real-time estimation of C is necessary for achieving an accurate displacement reconstruction.

B. Characterization of SMI Waveforms

In order to work out a technique for accurate displacement measurement, we studied the characteristics of an SMS associated with an SMI-based displacement sensing system by means of computer simulations. In the simulations we assume that the external target is subject to a simple harmonic vibration with $L(n) = L_0 + \Delta L \cos(2\pi \frac{f}{f_s} n)$, where L_0 is the initial distance between the LD surface and the target, f is the vibration frequency, and f_s is the sampling frequency. Values of these parameters are chosen as $L_0 = 0.24\,\text{m}$, $\Delta L = 1.37\,\mu\text{m}$, $f = 100\,\text{Hz}$, and $f_s = 51200\,\text{Hz}$. Based on these parameters, we generated SMS waveforms using the theoretical model in Eqs. (1)–(4), incorporating various vales of α and C. Figure 1(b) shows the SMS waveform for the case where $C = 3$ and $\alpha = 3$. We can see that each individual fringe on the SMS corresponds to a 2π phase change of $\phi_F(n)$, which is equivalent to $\lambda_0/2$ displacement of the external target. Also, fringes on

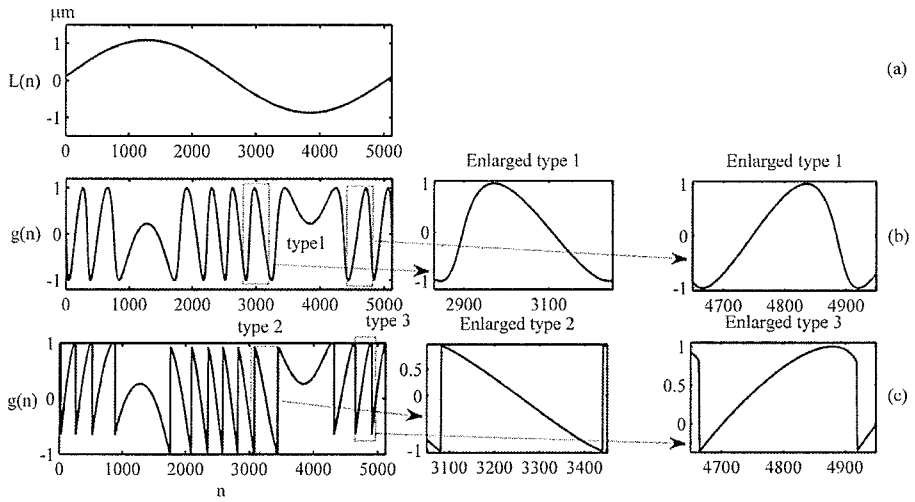

Fig. 2. Classification of fringe shapes. (a) Displacement waveform $L(n)$; (b) sinusoidal-like fringe (type 1) with $C = 0.5$, $\alpha = 3$; (c) left-inclined sawtoothlike fringe (type 2) and right-inclined sawtoothlike fringe (type 3) with $C = 2$, $\alpha = 3$.

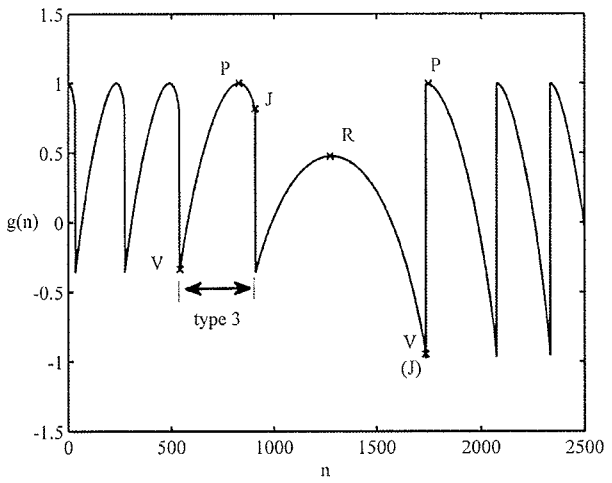

Fig. 3. Characteristic points on an SMS ($C = 2$, $\alpha = 1.3$).

the SMS are left-inclined when $L(n)$ decreases (the target moves toward the LD), and they are right-inclined when $L(n)$ increases (the target moves away from the LD).

In order to investigate the characteristics of SMS waveforms, extensive simulations were carried out using different values of α and C. The results show that SMS waveforms can be classified into three types (as shown in Fig. 2), including sinusoidal-like fringes (type 1), left-inclined sawtoothlike fringes (type 2), and right-inclined sawtooth fringes (type 3). Type 1 fringes occur in a weak feedback level where $C < 1$ [as shown in Fig. 2(b)]. Types 2 and 3 are observed in moderate or high feedback levels where $C > 1$ [as shown in Fig. 2(c)].

Let us consider the fringe shape of Type 3 by plotting a segment of Type 3 fringe in Fig. 3. We can see that there are four characteristic points on the segment (marked by R, P, V, and J), which describe the features of an SMS. R is called "reverse point," as it is the moment when the target changes its movement direction. P and V are called the "peak point" and "valley point," respectively, denoting the maximum and minimum points on each fringe. J is referred to as the "jumping point," on which an SMS exhibits a sudden change. Obviously, Type 1 fringes do not have jumping points. On a Type 2 fringe, the peak point P and a jumping point J merge together as the same point. Hence Types 1 and 2 can be considered special cases of Type 3.

C. Novel Approach

Given the discussion above, we present a novel algorithm for obtaining an accurate $\phi_F(n)$ and real-time C estimation.

1. *Obtaining Accurate Feedback Phase $\phi_F(n)$*

In order to obtain $\phi_F(n)$ accurately, an SMS should be segmented correctly. To this end we use the characteristic points described in Section 2.B. Hence, the first step is to locate these points from an SMS.

Locating the jumping points J and the reverse points R: In order to locate reverse points, we first differentiate an SMS $g(n)$ [shown in Fig. 4(a)] and then reshape the differentiated signal to obtain a pulse train $e(n)$ [shown in Fig. 4(b)], which clearly indicate the locations of all jumping points J.

In order to locate the reverse point R, we use $e(n)$ to find out a segment of the SMI waveform that

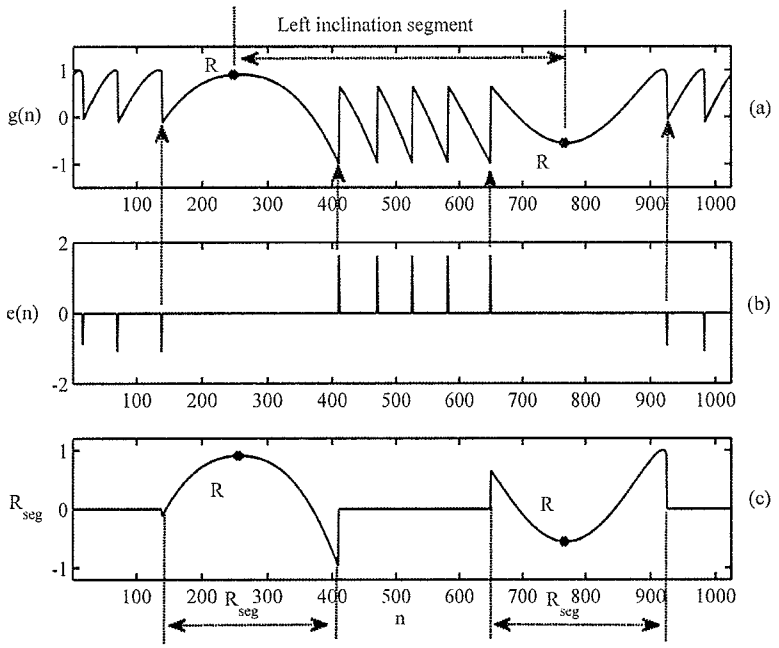

Fig. 4. Extracting reverse segments from an SMS. (a) SMS with $C = 3$, $\alpha = 3$; (b) pulse train $e(n)$; (c) extracted reverse segments of the SMS.

covers point R, and such a segment is marked by R_{seg}, as shown in Fig. 4(c). Obviously, the reverse point is the maximum or minimum point on the segment and hence can be easily located. Obviously, these reverse points R also divide the SMS waveform into segments. Two adjacent segments correspond to a complete object vibration cycle, over which we have two reverse points, indicating the starting and ending of the segment, and another reverse point marking the change from right-inclined fringes to left-inclined fringes, or vice versa. As shown by Figs. 4(a) and 4(b), $e(n)$ exhibits negative pulses on the right-inclined segment and positive pulses on the left-inclined segment, and hence its value can be used to identify these two types of segments.

With the above we are able to divide an SMS waveform into segments by means of the reverse points. Each two successive segments (a right-inclined one followed by a left-inclined one) correspond to a complete target vibration cycle. Without loss of generality, in the following we will consider displacement reconstruction using a two successive segment SMS.

Locating peak points P and valley points V: Now we divide the above selected segment into small pieces, each containing an individual fringe. This can be done by looking at the jumping points as shown in Fig. 5 when $C > 1$. The period structure of the waveform also enables us to achieve the same when $C < 1$. Over each individual fringe, we can locate the peak point and the valley point, which are the highest and the lowest points, respectively.

Calculation of $\phi_F(n)$: With all the characteristic points (that is, P, V, and J) located on every fringe segment, we use variables $p(k)$, $v(k)$, and $j(k)$, respectively, to store the locations of P, V, and J, where k is the fringe number index (that is, kth fringe). Then we apply the inverse cosine function to the segment of an SMS obtained above to get a wrapped phase denoted by $\phi_F^r(n)$, that is:

$$\phi_F^r(n) = \arccos(g(n)). \tag{5}$$

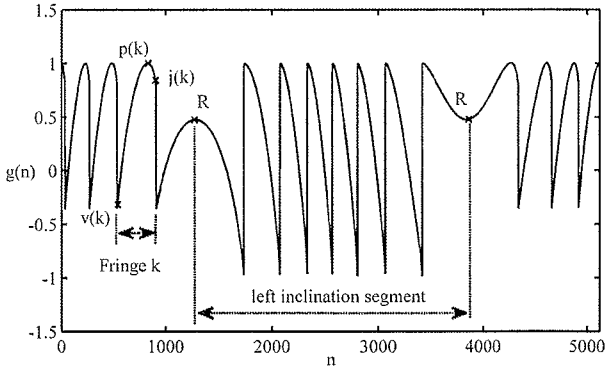

Fig. 5. Segmentation of an SMS with $C = 3$, $\alpha = 3$.

$\phi_F(n)$ is reconstructed on a fringe-by-fringe basis over the whole segment. Without loss of generality, we assume that there are K fringes on each half of the segment, and we start from the first fringe and then proceed to the next. We can also assume that $\phi_F(n)$ is the same as $\phi_F^r(n)$ for the first fringe period, and hence unwrapping is not required. $\phi_F(n)$ can be obtained by the following, depending on the different levels of optical feedback.

Let us consider the case of weak optical feedback (i.e., $C < 1$). As the SMS waveform is characterized by type 1 fringe patterns, only peak (P) and valley (V) points are observed. Considering the kth fringe period, we can use the following to recover $\phi_F(n)$ for the right-inclined part of the SMS waveform:

$$\phi_F(n) = \begin{cases} \phi_F^r(n) + 2\pi(k-1), & \text{when} \quad v(k) \le n < p(k) \\ -\phi_F^r(n) + 2\pi(k-1), & \text{when} \quad p(k) \le n < v(k+1) \end{cases}, \tag{6}$$

where k is the fringe number and $k = 1, 2, ..., K$. For the left-inclined part, we have the following:

$$\phi_F(n) = \begin{cases} \phi_F^r(n) - 2\pi(K-k+1), & \text{when} \quad v(k) \le n < p(k) \\ -\phi_F^r(n) - 2\pi(K-k+1), & \text{when} \quad p(k) \le n < v(k+1) \end{cases}, \tag{7}$$

where $k = 1, 2, ..., K$.

For moderate and strong feedback levels where $C > 1$, as shown by Fig. 3, type 2 and 3 fringe patterns are observed, which are left-inclined and right-inclined, respectively. Let us look at the type 3 part first. From Fig. 3 we can see that each individual fringe has two monotonic segments marked by VP and PJ. In other words, the SMS increases from point V to point P and then exhibits a short period of decrease to reach point J. Obviously, $\phi_F(n)$ should be calculated respectively over these two regions using the inverse cosine operation according to Eq. (3); that is:

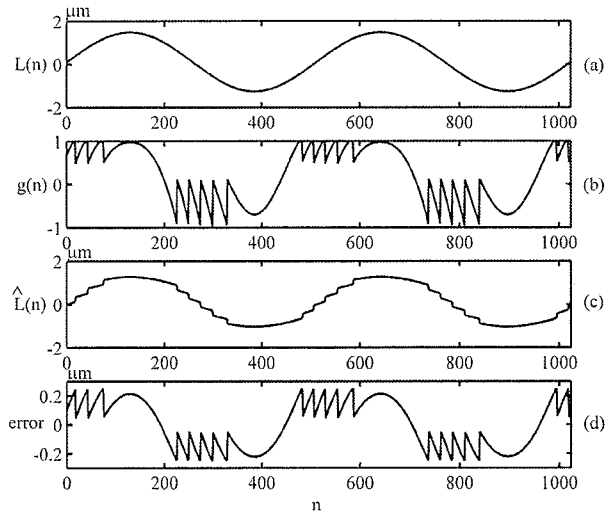

Fig. 6. Reconstruction result by using a preset $\hat{C}$ with $\hat{C} = 2$. (a) Displacement $L(n)$; (b) SMS with $C = 6$, $\alpha = 3$; (c) reconstructed displacement $\hat{L}(n)$ with $\hat{C} = 2$; (d) residual error between $L(n)$ and $\hat{L}(n)$.

$$\phi_F(n) = \begin{cases} \phi_F^r(n) + 2\pi(k-1), & \text{when } v(k) \le n < p(k) \\ -\phi_F^r(n) + 2\pi(k-1), & \text{when } p(k) \le n < j(k) \end{cases}, \tag{8}$$

where $k = 1, 2, ..., K$. For the left-inclined part (type 2) of the SMS waveform, we use the following:

2. *Estimation of Parameter C*

Once $\phi_F(n)$ is obtained accurately, we can calculate $\phi_0(n)$ using Eq. (2). However, parameters α and C must be available. Although α is generally considered a constant and its value can be accurately obtained using the methods in [16–19], C varies significantly during the operation of an SMI system [16,18], and real-time estimation of C is necessary for achieving an accurate displacement reconstruction. If a preset $\hat{C}$ different from the true value is used for displacement reconstruction, the reconstruction error can be significant. In order to look into the influence of C, we carried out computer simulations using the SMS waveforms obtained in Section 2.B. Figure 6 shows the results where the true value of C is 6 and a preset value $\hat{C} = 2$ is used to reconstruct $L(n)$. The maximum reconstruction error is $0.3\,\mu$m, which is clearly significant. Unfortunately, none of the existing techniques, such as those described in [10,11,13], estimate C value in real time and incorporate the estimate for displacement reconstruction.

In order to estimate the value of C, we assume that the displacement is smooth in nature, in which case, when an incorrect C value is employed to reconstruct the displacement, the result $\hat{L}(n)$ will exhibit fluctuation or discontinuity, which can be employed as a measure of the deviation of C from the true value. In order to confirm the effectiveness of such an idea, we differentiate the reconstructed $\hat{L}(n)$ and pass the result $D(n)$ through a high-pass filter, yielding $D_F(n)$,

$$\phi_F(n) = \begin{cases} \phi_F^r(n) - 2\pi(K-k+1), & \text{when } v(k) \le n < p(k)+1 \\ -\phi_F^r(n) - 2\pi(K-k+1), & \text{when } p(k)+1 \le n < j(k) \end{cases}. \tag{9}$$

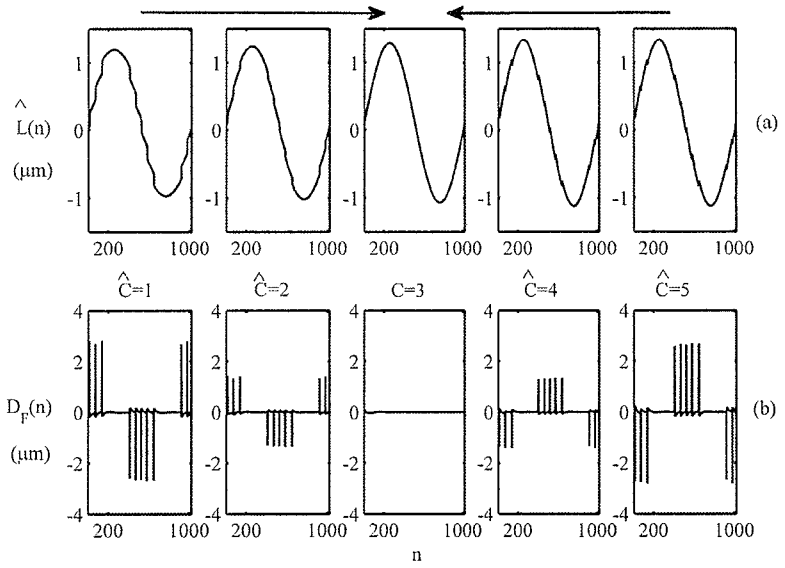

Fig. 7. Displacement reconstruction results and their corresponding fluctuation signals using different $\hat{C}$. (a) Displacement reconstruction result $\hat{L}(n)$, (b) fluctuation signals $D_F(n)$.

which is referred to as the fluctuation sequence. Figure 7 shows reconstruction results and the fluctuation signals $D_F(n)$ corresponding to different values of $\hat{C}$. We can see that the closer the $\hat{C}$ is to the true value of C, the smaller the magnitude of $D_F(n)$. Also, for the right-inclined part, $D_F(n)$ is positive when $\hat{C}$ is smaller than the true value of C, and $D_F(n)$ is negative when $\hat{C}$ is greater than the true value of C. On the left-inclined part, $D_F(n)$ is positive when $\hat{C}$ is greater than the true value of C, and it is negative when $\hat{C}$ is smaller than the true value of C. Hence we can always use the following to evaluate $\hat{C}$ in relation to the true value:

$$S = \sum D_F(n). \tag{10}$$

We will determine the true value of C by an iterative procedure. Initially, we assume that C is in the range $[C_{\min}, C_{\max}]$; for example, we can choose $C_{\max}$ and $C_{\min}$ to be 9.0 and 0.5, respectively, which should cover all practical situations.

When the range is given, we set the middle value as the estimate, that is, $\hat{C} = (C_{\max} + C_{\min})/2$. Then we will calculate $\phi_0(n)$, $\hat{L}(n)$, $D_F(n)$, and S using the approaches described above. We use a small positive number, ε, to test if $\hat{C}$ is close enough to the true value. In other words, if $|S| < \varepsilon$, we consider $\hat{C}$ the result of the estimation of the C value. Otherwise, the range of C will be updated iteratively as follows:

- For right-inclined SMS segments, we replace $C_{\min}$ by $\hat{C}$ if $S > \varepsilon$, or we replace $C_{\max}$ by $\hat{C}$ if $S < -\varepsilon$.
- For left-inclined SMS segments, we replace $C_{\max}$ by $\hat{C}$ if $S > \varepsilon$, or we replace $C_{\min}$ by $\hat{C}$ if $S < -\varepsilon$.

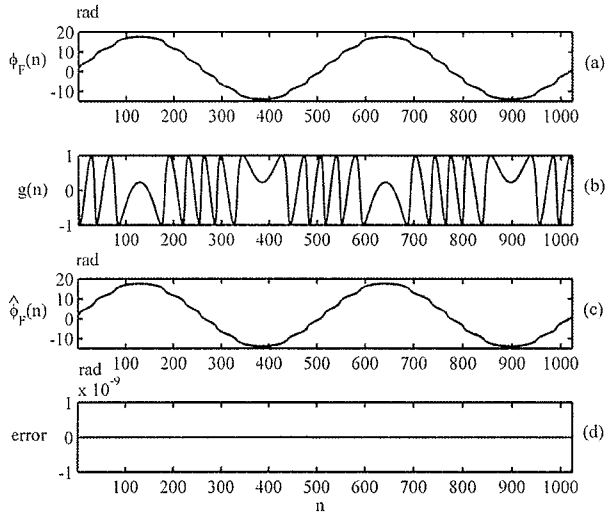

Fig. 8. Reconstruction results under a weak feedback level. (a) Feedback phase $\phi_F(n)$; (b) simulated SMS with $C = 0.6$, $\alpha = 2$; (c) reconstructed $\hat{\phi}_F(n)$; (d) residual error between $\phi_F(n)$ and $\hat{\phi}_F(n)$.

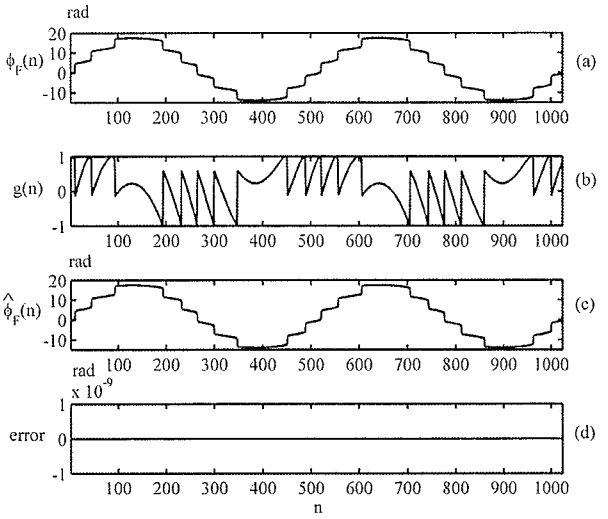

Fig. 9. Reconstruction results under a moderate feedback level. (a) Feedback phase $\phi_F(n)$; (b) simulated SMS with $C = 2$, $\alpha = 3$; (c) reconstructed $\hat{\phi}_F(n)$; (d) residual error between $\phi_F(n)$ and $\hat{\phi}_F(n)$.

The above updating process will continue until $|S| < \varepsilon$, and then we take $\hat{C} = (C_{\max} + C_{\min})/2$ as the result of the estimation.

3. Verification of the Proposed Approach

A. Computer Simulations

1. *Verification on $\phi_F(n)$.*

We generate SMS data using the same approach described in Section 2.B. In order to test the accuracy of the $\phi_F(n)$ calculation, we generated three segments of SMSes and their corresponding feedback phase

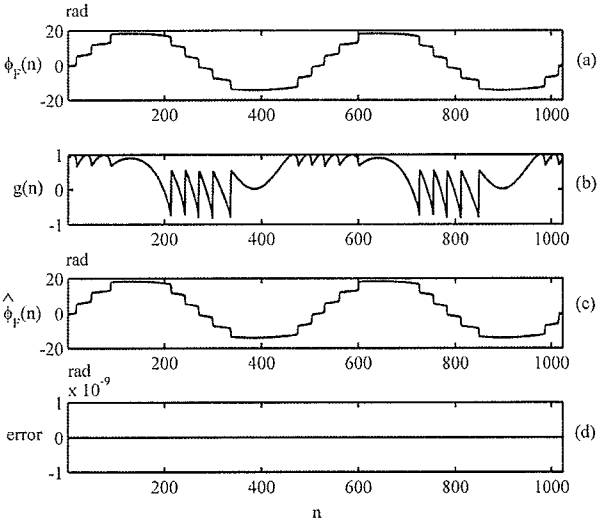

Fig. 10. Reconstruction results under a strong feedback level. (a) Feedback phase $\phi_F(n)$; (b) simulated SMS with $C = 5$, $\alpha = 1.3$; (c) reconstructed $\hat{\phi}_F(n)$; (d) residual error between $\phi_F(n)$ and $\hat{\phi}_F(n)$.

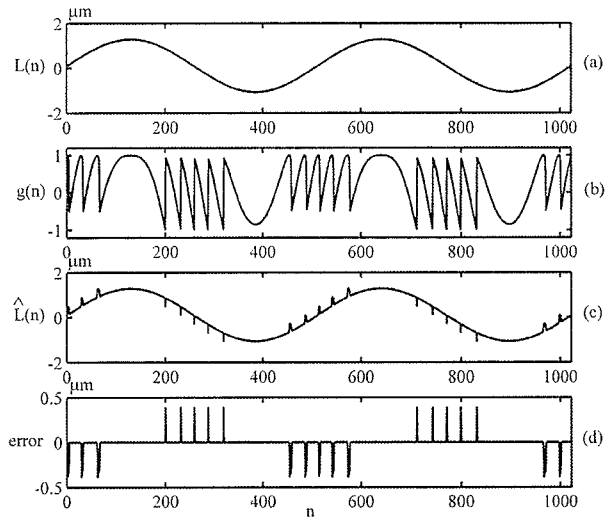

Fig. 11. Numerical simulation results when treating P and J as same point. (a) Displacement waveform $L(n)$; (b) SMS with $C = 2$, $\alpha = 4$; (c) reconstructed displacement $\hat{L}(n)$ from the SMS; (d) residual error between $L(n)$ and $\hat{L}(n)$.

$\phi_F(n)$ under different feedback levels. Figures 8–10 show the reconstruction results by the proposed reconstruction algorithm. We can see that the reconstruction error of $\phi_F(n)$ is negligible for all the cases considered. Therefore, we can say the proposed algorithm is able to accurately obtain $\phi_F(n)$.

The above results show that with an accurate C value, accurate displacement measurement can be achieved using $\phi_F(n)$ obtained by the proposed approach. Based on this, we are able to look into the technique presented in [7,10,13] and find out the reason for the errors as shown by the results presented in Figs. 2 and 3 in [7], Figs. 3 and 8 in [10], and Fig. 9 in [13]. After careful analysis of the reconstructed results, we believe that the errors come from the mistake where points P and J are treated as the same

Table 2. C Estimation Results

Actual C	Estimated $\hat{C}$	Error	Iteration Steps
0.7	0.6914	0.0086	8
1.5	1.4995	0.0005	9
3	2.9980	0.0020	7
5	4.9961	0.0039	6
8	8.0039	0.0039	6

point in [10]. In order to verify this, we carried out simulations by treating P and J as the same point, and Fig. 11 shows the results of the simulation. $L(n)$ and $\hat{L}(n)$ represent, respectively, original displacement and reconstructed displacement from an SMS. We can see that the error associated with $\hat{L}(n)$ can be up to 0.5 μm, which is significant. Also, the error in $\hat{L}(n)$ is similar to the result presented in [10] (Fig. 8 in [10]). Therefore, we can say that the algorithm in [10] ignored section PJ on an SMS and hence was not able to obtain accurate $\phi_F(n)$ for displacement reconstruction.

2. *Verification for C Measurement.*

After obtaining the feedback phase $\phi_F(n)$ without deviation, we use $\phi_F(n)$ to estimate C using the method described in Section 2.C.2. Without loss of generality, the searching range of C can be set as $[0.5, 9]$. A high-pass filter with cutoff frequency of 500 Hz is used for obtaining $D_F(n)$. Table 2 shows the results of the proposed method, where $\varepsilon = 0.0001$. We can see that with fewer than 10 iterations, C can be determined with accuracy of 98.77%, which is very fast.

It might be argued that the above approach is based on the assumption of smooth target movement, and accurate $L(n)$ can be obtained by simply passing the $\hat{L}(n)$ obtained with inaccurate C through a smooth filter. We studied the feasibility of using this idea, but found that it is not effective. This can been

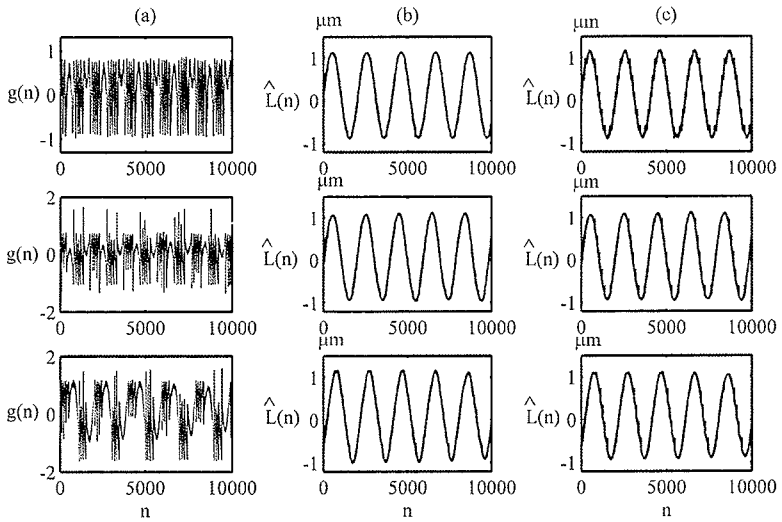

Fig. 12. Displacement reconstruction results by using experimental data. (a) Three SMSs under different feedback levels, (b) displacement reconstruction results cooperating real-time C values, (c) displacement reconstruction results with a preset C ($C = 5$).

seen by the simulation results in Fig. 6, where the true value of C is 6 and but $\hat{C} = 2$ is used to reconstruct displacement. The resulting $\hat{L}(n)$ not only contains sharp changes and discontinuity, but also suffers from slow-varying distortion, which cannot be removed by a simple "deglitching" algorithm or a smooth filter on $\hat{L}(n)$.

B. Experiment Verification

The proposed technique has also been verified with experimental data acquired in our laboratory. The experimental setup is shown in Fig. 1(c), where the target is a metal plate that vibrates in a simple harmonic form by placing it close to a loudspeaker. The LD used is provided by Thorlabs Company, model HL7851, which is biased with a dc current of 80 mA and operates at single mode. The temperature of the LD is maintained at 25 °C ± 0.1 °C by a temperature controller. The driving signal to the loudspeaker is sinusoidal and kept unchanged through the whole experimental process.

We acquired a number of SMSes under three different feedback levels and applied the proposed displacement reconstruction algorithm to these SMSes. The reconstruction results are shown in Fig. 12. The left column shows three different SMS segments. The middle column shows the reconstruction results with real-time estimated C values. For comparison purposes, reconstructed results using a preset C value ($\hat{C} = 5$) are shown in the right column. It is seen that a smooth displacement always uses the proposed algorithm with real-time C estimation; also, the constructed $\hat{L}(n)$ is proportional to the driving signal. However, if we use a preset C value to reconstruct displacement, the reconstructed results [as shown in Fig. 12(c)] contain fluctuations. Therefore we can say that the proposed approach is characterized by improved accuracy performance in contrast to existing techniques.

4. Conclusion

In this paper, we propose a technique to improve measurement performance for an SMI-based displacement sensing system. We achieved the improvement by the proposal of a new procedure for accurately determining the phase signal $\phi_F(n)$ from its wrapped version and a novel method for estimating the optical feedback parameter C in real time. We also identified the source of an error inherent to most existing displacement reconstruction methods, which is eradicated by the proposed technique. Both computer simulations and experiment have been used to verify the proposed algorithm, showing that displacement information can be accurately reconstructed.

References

1. G. Giuliani, M. Norgia, S. Donati, and T. Bosch, "Laser diode self-mixing technique for sensing applications," J. Opt. A: Pure Appl. Opt. **4**, S283–S294 (2002).
2. T. Bosch, "An overview of self-mixing sensing applications," in *Proceedings of IEEE Conference on Optoelectronic and Microelectronic Materials and Devices* (IEEE, 2004), pp. 385–392.
3. L. Scalise, Y. Yanguang, G. Giuliani, G. Plantier, and T. Bosch, "Self-mixing laser diode velocimetry: application to vibration and velocity measurement," IEEE Trans. Instrum. Meas. **53**, 223–232 (2004).
4. S. Donati, M. Norgia, and G. Giuliani, "A review of self-mixing techniques for sensing applications," in *Proceedings of the 17th Annual Meeting of the IEEE Lasers and Electro-Optics Society, 2004 (LEOS 2004)*, Vol. 261, pp. 260–261.
5. S. Donati, "Laser interferometry by induced modulation of cavity field," J. Appl. Phys. **49**, 495–497 (1978).
6. S. Donati, G. Giuliani, and S. Merlo, "Laser diode feedback interferometer for measurement of displacements without ambiguity," IEEE J. Quantum Electron. **31**, 113–119 (1995).
7. S. Merlo and S. Donati, "Reconstruction of displacement waveforms with a single-channel laser-diode feedback interferometer," IEEE J. Quantum Electron. **33**, 527–531 (1997).
8. N. Servagent, F. Gouaux, and T. Bosch, "Measurements of displacement using the self-mixing interference in a laser diode," J. Opt. **29**, 168–173 (1998).
9. D. M. Guo, M. Wang, and S. Q. Tan, "Self-mixing interferometer based on sinusoidal phase modulating technique," Opt. Express **13**, 1537–1543 (2005).
10. G. Plantier, C. Bes, T. Bosch, and F. Bony, "Autoadaptive signal processing of a laser diode self-mixing displacement sensor," in *Proceedings of IEEE Conference on Instrumentation and Measurement Technology* (IEEE, 2005), pp. 1013–1017.
11. C. Bes, G. Plantier, and T. Bosch, "Displacement measurements using a self-mixing laser diode under moderate feedback," IEEE Trans. Instrum. Meas. **55**, 1101–1105 (2006).
12. U. Zabit, T. Bosch, and F. Bony, "A fast derivative-less optimization of the feedback coupling coefficient for a self-mixing laser displacement sensor," in *Proceedings of IEEE North-East Workshop on Circuits and Systems and TAISA* (IEEE, 2009), pp. 1–4.
13. U. Zabit, T. Bosch, and F. Bony, "Adaptive transition detection algorithm for a self-mixing displacement sensor," IEEE Sens. J. **9**, 1879–1886 (2009).
14. R. Lang and K. Kobayashi, "External optical feedback effects on semiconductor injection laser properties," IEEE J. Quantum Electron. **16**, 347–355 (1980).
15. N. Schunk and K. Petermann, "Numerical analysis of the feedback regimes for a single-mode semiconductor laser with external feedback," IEEE J. Quantum Electron. **24**, 1242–1247 (1988).
16. Y. Yu, G. Giuliani, and S. Donati, "Measurement of the linewidth enhancement factor of semiconductor lasers based on the optical feedback self-mixing effect," IEEE Photon. Technol. Lett. **16**, 990–992 (2004).
17. J. Xi, Y. Yu, J. F. Chicharo, and T. Bosch, "Estimating the parameters of semiconductor lasers based on weak optical feedback self-mixing interferometry," IEEE J. Quantum Electron. **41**, 1058–1064 (2005).
18. Y. Yu, J. Xi, J. F. Chicharo, and T. M. Bosch, "Optical feedback self-mixing interferometry with a large feedback factor C: behavior studies," IEEE J. Quantum Electron. **45**, 840–848 (2009).
19. Y. Yu, J. Xi, J. F. Chicharo, and T. Bosch, "Toward automatic measurement of the linewidth-enhancement factor using optical feedback self-mixing interferometry with weak optical feedback," IEEE J. Quantum Electron. **43**, 527–534 (2007).